THE JOURNAL OF BIOLOGICAL CHEMISTRY VOL. 285, NO. 48, pp. 37693–37703, November 26, 2010

The Novel PMCA2 Pump Mutation *Tommy* Impairs Cytosolic Calcium Clearance in Hair Cells and Links to Deafness in Mice*

Received for publication, July 30, 2010, and in revised form, September 3, 2010 Published, JBC Papers in Press, September 8, 2010, DOI 10.1074/jbc.M110.170092

Mario Bortolozzi[‡§1], Marisa Brini[¶1], Nick Parkinson[‖1,2], Giulia Crispino[§], Pietro Scimemi[**], Romolo Daniele De Siati[**], Francesca Di Leva[¶3], Andrew Parker[‖], Saida Ortolano[§4], Edoardo Arslan[**], Steve D. Brown[‖5], Ernesto Carafoli[§5], and Fabio Mammano[‡§5,6]

*From the [‡]Department of Physics "G. Galilei," University of Padua, Padua 35131, Italy, the [§]Venetian Institute of Molecular Medicine, Padua 35129, Italy, the [¶]Department of Biological Chemistry, University of Padua, Padua 35121, Italy, the [‖]MRC Mammalian Genetics Unit, MRC Harwell, Oxfordshire OX11 0RD, United Kingdom, and the **Department of Medical and Surgical Specialities-Audiology and Phoniatric Service, University of Padua, Padua 35128, Italy*

The mechanotransduction process in hair cells in the inner ear is associated with the influx of calcium from the endolymph. Calcium is exported back to the endolymph via the splice variant *w/a* of the PMCA2 of the stereocilia membrane. To further investigate the role of the pump, we have identified and characterized a novel ENU-induced mouse mutation, *Tommy*, in the PMCA2 gene. The mutation causes a non-conservative E629K change in the second intracellular loop of the pump that harbors the active site. Tommy mice show profound hearing impairment from P18, with significant differences in hearing thresholds between wild type and heterozygotes. Expression of mutant PMCA2 in CHO cells shows calcium extrusion impairment; specifically, the long term, non-stimulated calcium extrusion activity of the pump is inhibited. Calcium extrusion was investigated directly in neonatal organotypic cultures of the utricle sensory epithelium in *Tommy* mice. Confocal imaging combined with flash photolysis of caged calcium showed impairment of calcium export in both *Tommy* heterozygotes and homozygotes. Immunofluorescence studies of the organ of Corti in homozygous *Tommy* mice showed a progressive base to apex degeneration of hair cells after P40. Our results on the *Tommy* mutation along with previously observed interactions between cadherin-23 and PMCA2 mutations in mouse and humans underline the importance of maintaining the appropriate calcium concentrations in the endolymph to control the rigidity of cadherin and ensure the function of intersterecilia links, including tip links, of the stereocilia bundle.

Deflection of the stereocilia bundle that protrudes from hair cells into the endolymph causes the opening of mechanotransduction (MET)[7] channels and influx of K^+ and Ca^{2+} into the cells, ensuing in graded changes of the resting membrane potential (*i.e.* in a receptor potential) (1). Outer hair cells (OHC) of the mammalian cochlea are mechanosensors that, acting as motor cells (2, 3), produce forces driven by their receptor potential and amplify the mechanical vibrations of the basilar membrane in response to sound (4, 5). The amplification action activates the MET process in inner hair cells and consequent release of neurotransmitter to afferent dendrites of spiral ganglion neurons whose action potentials relay acoustic information to the central nervous system (6).

In all types of hair cells, MET channels are gated by tension applied through extracellular tip links, which are oriented along the main symmetry axis of the hair bundle from the apex of one stereocilium to the lateral wall of its taller neighbor (7). Recent work (8) has confirmed that MET channels are located at the lower end of the tip link, in the two shorter rows of stereocilia (9). Earlier experiments performed under non-physiological conditions of Ca^{2+} concentrations (mM range) showed that ~90% of the MET current was carried by K^+ and 10% by Ca^{2+} (10). More recent work has indicated that the fraction of MET current carried by Ca^{2+} decreases directly in proportion to its external concentration, accounting for only ~0.2% of the current in a saline comparable with endolymph (11), in which the Ca^{2+} concentration (~20 μM) is about 100-fold lower that in all other extracellular fluids (12). The entry of Ca^{2+} has so far been considered vital for adaptation of the mechanotransduction process (1), but these concepts may now have to be revised (11).

Ca^{2+} entering through MET channels is rapidly buffered by endogenous mobile chelators, *e.g.* parvalbumin (13). However, Ca^{2+} must be eventually exported back to the endolymph by the PMCA pump, which is highly concentrated in the stereocilia plasma membrane (11, 14, 15). The pump isoform of the stereocilia, PMCA2, which is coded by the *ATP2b2* gene, is known to be essential for hearing and balance (15–18). PMCA2 has properties that set it apart from all other PMCAs (19); it has very high affinity for the activator calmodulin, yet its activity is only modestly activated by it (19, 20). Unlike the other three

* This work was supported by the European Commission under the Sixth Research Frame Program of the European Union (FP6 Integrated Project EuroHear, Grant LSHGCT20054512063) (to F. M., E. C., and S. D. B.), by the Fondazione Cariparo (Progetti di Eccellenza 2006–2007), Telethon Italy Grant GGP09137, by the Italian Ministry of Research (PRIN 2007, Grant 2007BZ4RX3_003) (to F. M.), and by Telethon Foundation Grant GGP04169 and the Italian Ministry of University and Research (PRIN 2005) (to M. Brini).
⌘ *Author's Choice*—Final version full access.
[1] These authors are joint first authors.
[2] Present address: Systems Biology Laboratory, Abingdon, UK.
[3] Present address: CIBIO, University of Trento, Trento 38123, Italy.
[4] Present address: Neuropathology, Patological Anatomy Department, University Hospital of Vigo, Vigo 36203, Spain.
[5] Both are senior authors.
[6] To whom correspondence should be addressed: via G. Orus 2, 35129, Padova, Italy. E-mail: fabio.mammano@unipd.it.

[7] The abbreviations used are: MET, mechantransduction; OHC, outer hair cell; ABR, auditory brainstem response; SERCA, sarco(endo)plasmic reticulum calcium ATPase; DPBS, Dulbecco's PBS; UC, utricle cultures; CS, cochlear slices; PMCA, plasma membrance Ca^{2+} ATPase; ENU, *N*-ethyl-*N*-nitrosourea; mRFP, monomeric red fluorescent protein.

PMCA basic isoforms, PMCA2 has peculiarly high activity in the absence of the activator calmodulin, *i.e.* it pumps Ca^{2+} out of cells at a relatively high constant rate.

All PMCA transcripts undergo alternative splicing at site A in the cytosolic loop connecting transmembrane domains 2 and 3 and at site C in the cytosolic tail of the pump. The splicing process is uniquely complex in PMCA2, as it involves the insertion of up to three exons at site A and of two at site C. The site A inserts are in-frame and generate variant *w* when all three exons are inserted; those at site C create instead a novel stop codon, truncating the pump prematurely and generating variant *a*. Recent work has conclusively shown that splicing at site A dictates apical targeting in hair cells for PMCA2 and that the rodent hair-bundle isoform is variant PMCA2*w/a*; the basolateral plasma membrane of the hair cell contains instead PMCA1 (21, 22). Tests of the activity of the various PMCA2s expressed in model cells have revealed a decreased ability of the *w/a* variant to control incoming Ca^{2+} pulses in comparison to the non inserted *z/b* variant (23), which, as mentioned, responds with a lower activation to the arrival of Ca^{2+} pulses with respect to the ubiquitous PMCA1 or PMCA4 pumps (19). The stereocilia of vestibular hair cells and OHCs are the only plasma membrane in which the *w/a* variant of PMCA2 has so far been detected in mammals (21). The unusually low concentration of Ca^{2+} in the endolymph that bathes them (12) has evidently led to the evolutionary selection of a PMCA variant with the peculiar Ca^{2+} exporting properties of PMCA2*w/a*.

It has been known for more than a decade that ablation of the *ATP2b2* gene produces hereditary deafness in mice (15). PMCA2 mutations were then discovered linked to recessively inherited deafness in mice (17, 18, 24–26) and humans (23, 27). In the present contribution we describe PMCA2 mutant *Tommy* mice that exhibit a profound deafness phenotype (48). The mutation affects a highly conserved residue located next to the active site in the cytosolic loop that connects transmembrane domains 4 and 5 of the enzyme. This residue is classified as E584 in the *z/b* variant of the PMCA2 but corresponds to E629 in the PMCA2*w/a* variant due to the 45-amino acid site A insertion in the first intracellular loop. The analysis of the defect in model cells overexpressing the mutated pump and in hair cells of organotypic utricular cultures has revealed a marked depression of the unstimulated, long term ability of the PMCA2*w/a* variant to export Ca^{2+} from the stereociliary cytosol.

EXPERIMENTAL PROCEDURES

Mice—All animals used for *Tommy* mutant line derivation were housed and maintained in the Mary Lyon Centre at MRC Harwell under specific pathogen-free conditions in individually ventilated cages with environmental conditions outlined in the Home Office Code of Practice. Animal procedures were carried out in line with Home Office regulations, and mice were euthanized by Home Office Schedule 1 methods. The *Tommy* mutant line was derived from a dominant ENU mutagenesis screen at the MRC MGU Harwell (28) in which BALB/c mice were treated with ENU and mated to C3H/HeH and F1 progeny subject to a variety of screening procedures.

All animals used for ABR recordings and fluorescence microscopy experiments were housed and maintained in the Venetian Institute of Molecular Medicine, Padua, Italy. The care and use of the animals were approved by the Animal Care and Use Committee of the University of Padua.

Click Box Screening—Mice were screened according to the SHIRPA protocol (28) and placed in the palm of the hand and tested with a click box (Institute of Hearing Research, Nottingham, UK), which produces a brief audio stimulus ~20 kHz tone at 90 db when held 30 cm away from the subject. Mice with unaffected hearing elicit the "preyer" response, a backwards flick of the ear pinnae. In most cases the preyer reflex is followed by startle response that can range from a contracting of the neck muscles to a rapid jump backwards. A lack of either of the responses was recorded as no response to the click box (29).

Genome Scan—We used a pooling strategy employing DNA from affected mice and genome-wide fluorescent simple sequence length polymorphism-based screening (28) to provide an initial map position for the *Tommy locus, Tmy,* to a 20-centimorgan region of chromosome 6 flanked by markers *D6Mit67* and *D6Mit295*. Additional polymorphic markers within the critical region were identified from public databases (microsatellite markers: Mouse Genome Informatics, Broad Institute Genetic Map of the Mouse Genome (Whitehead/MIT) and Center for Inherited Disease Research; single nucleotide polymorphism markers: Ensembl, Genomics Institute of the Novartis Research Foundation website) and were tested for polymorphism in the parental strains BALB/cAnN and C3H/HeH. For high resolution mapping, polymorphic microsatellite and single nucleotide polymorphism amplicons were analyzed on 6% acrylamide gels using the single-stranded conformational polymorphism method allowing the *Tmy* critical region to be reduced to a 6-centimorgan interval flanked by polymorphic microsatellite markers *D6Mit287* and *D6Mit150* and encompassing the *dfw* critical region.

In Vivo Recordings of Auditory Brainstem Response (ABR)—Mice aged between P18 and P90 were anesthetized with an intraperitoneal injection of zolazepam (25 mg/Kg) and xylazine (10 mg/kg). Supplemental doses were then administered as needed. Body temperature was kept at 38 °C by a feedback-controlled heating pad. Each recording procedure lasted up to 70 min. Acoustic stimuli were produced in the free field within a foam-padded, shielded acoustic chamber by a System 3 Real-time Signal Processing System (Tucker-Davis Technologies, Alachua, FL) combined with an ES1 electrostatic speaker mounted 4 cm in front of the mouse's ear. Stimuli consisted in tone bursts (1-ms rise/decay; 3-ms plateau) at 8, 14, 20, 26, and 32 kHz, and clicks (0.1 ms) delivered at a repetition rate of 13 Hz. A maximum of 100 db sound pressure level, was employed for all stimuli. To monitor electrical signals, a subdermal (active) needle electrode was inserted at the vertex, whereas ground and reference electrodes were inserted subdermally in the loose skin beneath the pinnae of opposite ears. Bioelectrical potentials were differentially amplified (50,000×), filtered (5–8,000 Hz), and digitized (25 μs) for averaging (AT MIO 16XE-10, Labview 7.0, National Instruments Corp., Austin, TX). ABR threshold was defined as the lowest step in a 10-db decremented scale at which the IV wave could be recognized by a trained Audiometry specialist. Judgment of threshold was confirmed by a second specialist. In case the IV wave of the ABR

could not be discerned in response to the maximum 100-db sound pressure level stimulus, a nominal threshold of 110 db sound pressure level was assigned.

Cloning and Mutagenesis of pmRFP-PMCA2w/a—mRFP was amplified from pCDNA3.1/zeo-mRFP (donated by Dr. M. Zaccolo, Padua, Italy) using the following primers: forward, 5′-GC**GCTAGC**ATGGCCTCCTCCGAGGACGTCA-3′, and reverse, 5′-GC**AGATCT**GAGGCGCCGGTGGAGTGGCGG-3′, bearing restriction sites for NheI and BglII, respectively (in bold). The PCR product was than digested with NheI and BglII and inserted in pEGFP-c1 (Clontech, Palo Alto, CA) digested with NheI and BglII to create pmRFP-c1. PMCA2 *w/a* in pMM2 (donated by Dr. E. Strehler, Rochester, MN) was excised by independent digestion with SalI-EcoRI and EcoRI-KpnI and inserted into XhoI-KpnI sites of pmRFP-c1 in a three-part ligation reaction resulting in pmRFP-PMCA2 *w/a*. The construct was controlled by sequencing. Site-directed mutagenesis was carried out to obtain the mutant cloned in the appropriate vector. pmRFP-PMCA2 *w/a* was used as the target, and experiments were performed according to the manufacturer's standard protocol (QuikChange, Stratagene, Cedar Creek, TX). The following primers were used: *Tommy* 5′-AGCAAAGGTGCTTCGAAGATTGTGCTCAAAA-3′ (forward) and 5′-TTTTGAGCACAATCTTCGAAGCACCTTTGCT-3′ (reverse). The nucleotide that determines the mutation is underscored.

Immunolocalization of Overexpressed Pumps and Membrane Fluorescence Computation—CHO cells were grown in Ham's F-12 medium supplemented with 10% fetal calf serum (FCS). Before transfection, they were seeded onto 13-mm glass coverslips and allowed to grow to 50% confluence. Transfection with 3 μg of plasmid DNA (or 1.5:1.5 μg in the case of co-transfection) was carried out with a calcium phosphate procedure (30). Immunocytochemistry quantified the expressed pump proteins in the plasma membrane of transfected cells. CHO cells expressing the PMCA2 variants were stained with polyclonal isoform-specific PMCA antibody 2N (Affinity Bioreagent, Inc., Golden, CO) or a monoclonal antibody recognizing all pump isoforms (5F10, Affinity Bioreagent) at a 1:100 dilution in PBS. Staining was carried out with Alexa 488-labeled anti-rabbit or anti-mouse secondary antibodies (Molecular Probes, Invitrogen) at a 1:50 dilution in PBS, and total fluorescence intensity in membrane was quantified using software developed in the Laboratory, as previously described (23, 25). For each construct, fluorescence was averaged over a total of 50 cells in 3 different slides.

Preparation of Membranes from CHO Cells, SDS-PAGE, and Western Blot Analysis—36 h after transfection CHO cells were washed twice with cold PBS buffer and scraped in lysis buffer (10 mM Tris-HCl (pH 8.0), 1 mM EDTA, 2 mM phenylmethylsulfonyl fluoride, and 1 mM dithiothreitol). After centrifugation at 1000 × *g* for 5 min, the cells were resuspended in 80 μl of lysis buffer and subjected to three cycles of freeze and thaw. The proteins of the lysates were quantified using the Bradford reagent (Sigma). 20 μg of proteins were loaded on 7.5% polyacrylamide gel and transferred to nitrocellulose membranes that were incubated with polyclonal PMCA2 antibody 2N (Sigma, diluted 1:1000) and monoclonal β-actin antibody (Sigma). After incubation with anti-rabbit horseradish peroxidize-conjugated secondary antibodies (Santa Cruz Biotechnology, Inc., Santa Cruz, CA), the blots were developed with ECL reagents (Amersham Biosciences). The quantitative analysis was carried out by densitometric analysis using the Kodak 1D Image Analysis program (Kodak Scientific Imaging System, New Haven, CT). Antibodies against β-actin were used to normalize the data obtained from the densitometric analyses.

Ca^{2+} Measurements with Recombinant Aequorin—Recombinant cytosolic aequorin, as produced inactive by CHO cell transfection, was reconstituted in functional chemiluminescent protein by incubating cells for 1–3 h with 5 μM prosthetic group coelenterazine in Dulbecco's modified Eagle's medium (DMEM) supplemented with 1% FCS at 37 °C in a 5% CO_2 atmosphere. Additions to the KRB medium (1 mM $CaCl_2$, 100 μM ATP) were made as specified in the legend of Fig. 5. The experiments and luminescence calibration into Ca^{2+} values were carried out according to Brini *et al.* (30). Data are reported as the mean ± S.D. Statistical differences were evaluated by Student's 2-tailed *t* test for unpaired samples. A p value <0.01 was considered statistically significant. We have previously shown that the contribution of the native endoplasmic reticulum Ca^{2+} pump (SERCA) to the reduction of Ca^{2+} level in the cytoplasm is marginal in cells that overexpress PMCA variants (23). SERCA pump inhibitors were, thus, not used in these experiments. Furthermore, by comparison with the results of control experiments performed in naive cells (not transfected with PMCA constructs), we determined that the recovery phase is dominated by the overexpressed PMCA2 pump. Similarly, the contribution of plasma membrane Ca^{2+} influx channels, opened by the emptying of intracellular stores, to the lowering of cytosolic Ca^{2+} was disregarded, assuming it would have been the same in all conditions tested.

Preparation of Organotypic Cultures from Utricle Sensory Epithelia—Utricles were excised from wild type, heterozygous, or homozygous *Tommy* mice between P6 and P7. Postnatal mice were decapitated for inner ear extraction, the otic capsule was opened medially in a dissection solution, and the utricle was extracted by micro forceps. The dissection saline was composed of Hanks' balanced salt solution (catalogue no. H6648; Sigma) with 10 mM Hepes, 10,000 units/liter penicillin, and 25 μg/liter Fungizone. The endolymphic compartment was cut open, and the otolithic membrane was removed by the flux of a syringe filled with saline. The utricle epithelium was fixed by Cell-Tak (BD Biosciences) mixed with 90% $NaHCO_3$ to the lateral side of a glass capillary (1.5 mm diameter, 5 mm length) that had been previously glued to a microscope slide by a small drop of Sylgard Silicon Elastomer (Dow Corning, Wiesbaden, Germany). The organs were preserved in culture for 1 day at 37 °C in a complete medium of 95% DMEM/Ham's F-12 (1:1) (with L-glutamine, without Hepes; Invitrogen) and 5% FBS.

Confocal Ca^{2+} Imaging Combined with Flash Photolysis of Caged Ca^{2+} in Hair Cells—At recording time, *i.e.* 1 day after dissection, utricle cultures were loaded with 10 μM Fluo-4 AM (Invitrogen) and 10 μM *o*-nitrophenyl-EGTA AM (Invitrogen) for 50 min at 37 °C in DMEM (Invitrogen) supplemented with 25 μM sulfinpyrazone and Pluronic F-127 (0.1%). For deesterification, cultures were superfused for 10 min with Hanks' balanced salt

solution (Invitrogen) supplemented with 4.5 g/liter glucose and 2 mM anhydrous $CaCl_2$ (pH 7.4, osmolality 330 mOsm) and transferred to a chamber mounted on the stage of an upright confocal system (Bio-Rad Radiance 2100) incorporating an Eclipse E600FN optical microscope (Nikon Instruments Europe B.V., 1183AS Amstelveen, The Netherlands) equipped with a water immersion objective (Fluor 60×, 1.0 N.A., Nikon).

Intracellular Fluo-4 fluorescence was excited by the 488-nm line of an argon-ion laser and selected around 528 nm by a HQ528/50m narrow-band interference filter. A rapid increase in cytosolic Ca^{2+} ($[Ca^{2+}]_i$) was achieved by the photorelease of Ca^{2+} from the Ca^{2+}-bound state of *o*-nitrophenyl-EGTA. The ultraviolet (UV) illumination used for Ca^{2+} uncaging covered an area of about 10,000 μm^2, comprising a few hair cells, and was generated by a 375-nm solid state laser connected to the microscope through a 600-nm-diameter optical fiber. The recollimated fiber output was reflected off a dichromatic beam splitter (400 DCLP, Chroma) positioned at 45° just above the microscope objective lens. UV light was delivered for 60 ms during the 40th frame (frame rate 7 Hz) under control of a transistor-transistor logic signal generated by a PC that monitored the frame trigger output of the confocal microscope. After obtaining readout for the Fluo-4 base-line fluorescence, f_0, in the hair cell, exposure to UV light generated a uniform Ca^{2+} transient distributed over the whole cell. Ca^{2+} concentration change was probed by the $\Delta f/f_0$ signal, defined as the percentage change of Fluo-4 fluorescence *f* relative to f_0 (31). Image sequences were stored on a disk and processed off-line as previously described (23, 25) using the Matlab 7.0 software package (The MathWorks, Inc., Natick, MA). Fluorescence traces were obtained by spatially averaging pixel signals within the stereociliary compartment of wild type heterozygous and homozygous *Tommy* mice. The parameter used to quantify the stereocilia ability to extrude Ca^{2+} was the decay time constant (τ) of the single-exponential curve fitting the first part of the $\Delta f/f_0$ trace after the UV flash.

Transversal and Horizontal Cochlear Section Preparation—Cochleae were dissected from P40 and P60 *Tommy* mice, fixed in 4% paraformaldehyde overnight, and decalcified for the next 3 days in Dulbecco's phosphate-buffered saline (DPBS, Invitrogen) with 0.3 M EDTA. After 3 washes in DPBS, cochleae were included in 3% agarose (dissolved in DPBS) and cut in 100-μm thickness slices either parallel or perpendicular to the modiolar axis (for transversal and horizontal sections, respectively). Sample orientation was controlled by a crossed pair of goniometers (Thorlabs GmbH, Dachau/Munich, Germany) coupled to a vibratome (VT 1000S, Leica Microsystems, Wetzlar, Germany). Section were cut with double-edge razor blades (Gillette Platinum) at speed 6 and frequency 6, both on a scale of 10 on the vibratome range.

Immunohistochemistry of PMCA2 in Hair Cells—Utricle cultures (UC) and cochlear slices (CS) were rinsed in DPBS containing 1% BSA (*rinse* solution). After permeabilization at room temperature with 0.1% Triton X-100 dissolved in 2% BSA solution (1 h for UC, 3 h for CS), PMCA2 was immunolabeled by overnight incubation at 4 °C with polyclonal isoform-specific PMCA antibody 2N (Thermo Scientific ABR, PA1-915) diluted in rinse solution (1:400). After washing 3 times in PBS (5 min each time for UC, 1 h for CS), the secondary antibody (Alexa Fluor 488 goat anti-rabbit IgG, Invitrogen) was applied at 5 μg/ml for 1 h at room temperature. Nuclei were stained by incubation (1 h for UC and overnight for CS) in 4′,6-diamidino-2-phenylindole dihydrochloride (DAPI, Invitrogen) diluted (5 μM) in rinse solution. The same procedure was used to stain F-actin by Texas Red-X phalloidin (Invitrogen) in CS. Membranes in UC were stained by 20 min of incubation in FM4-64FX (Invitrogen) diluted at 15 μM in DPBS. After washing for three times in DPBS, CS were mounted onto glass slides with a mounting medium (FluorSave™ Reagent, Merck KgaA, Darmstadt, Germany) and imaged with an inverted confocal microscope (TCS SP5, Leica Mikrosysteme Vertrieb GmbH) equipped with oil immersion objectives (Leica 40×,1.25 N.A., or Leica 63×, 1.4 N.A.). UC were imaged by an upright confocal system (Bio-Rad Radiance 2100 incorporating a Nikon Eclipse E600FN microscope) equipped with a water immersion objective (Nikon Fluor 60X, 1.0 N.A.). For CS, Alexa Fluor 488 was excited by the 488-nm line of an air-cooled argon-ion laser, and its fluorescence emission was collected in a spectral window between 495 and 540 nm. Texas Red was excited by the 561-nm line of a diode-pumped solid-state laser, and its emission was collected between 600 and 690 nm. DAPI was excited by the 405-nm line of a diode laser module (emission light was collected between 410 and 440 nm) or excited by a pulsed Tsunami laser (Spectra-Physics, Santa Clara, CA 95054) at 830 nm (emission light was collected with a HQ450/80 filter). For UC, Alexa Fluor 488 was excited by the 488-nm argon-ion laser of the Bio-Rad system, and its fluorescence emission was collected by using a HQ515/30 narrow-band interference filter. FM4-64 was excited by the same argon laser line and observed by a long pass interference filter E570LP.

RESULTS

Isolation and Initial Characterization of Tommy Mutants—The *Tommy (Tmy)* founder mouse was isolated from an aged cohort of BALB/c^{ENU}/C3H F1 mice produced during a dominant genome wide mutagenesis screen carried out by our facility (28). Mice from within this cohort were SHIRPA tested at 4 weeks postpartum, aged, then repeat SHIRPA-tested at 26 weeks. At 4 weeks of age the founder male exhibited a wild type ear flick preyer reflex response to a transient 20-kHz pure tone burst stimulus of ≈90 db sound pressure level emitted by a calibrated click box. At age 26 weeks no such reflex was observed with identical stimuli, indicating a profound deafness. No other phenotype was observed with SHIRPA at either age. The founder BALB/c^{ENU}/C3HF1-*Tmy*/$^+$ animal was backcrossed to C3H/HeH, then affected animals were successively backcrossed to C3H/HeH to maintain the colony. After confirmation of inheritance, progeny were repeatedly tested for the presence of a wild type hearing response using the click box assay. Profound deafness in *Tmy*/$^+$ animals was first observed at ~12 weeks of age and was nearly fully penetrant after 30 weeks. Middle and inner ear dissections of affected animals found no gross morphological defects of the cochlea, vestibular labyrinth, or ossicles. In addition no evidence was found of middle ear infection or disease (data not shown).

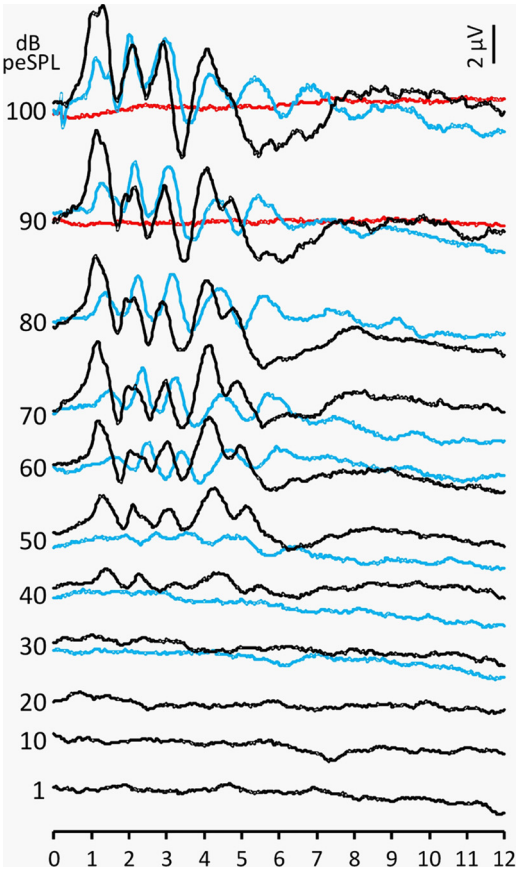

FIGURE 1. **Hearing thresholds measured by the ABR technique.** Representative ABR recordings in response to click stimuli from wild type (postnatal day 31, *black traces*), heterozygous (postnatal day 27, *blue traces*), and homozygous (postnatal day 24, *red traces*) *Tommy* mice.

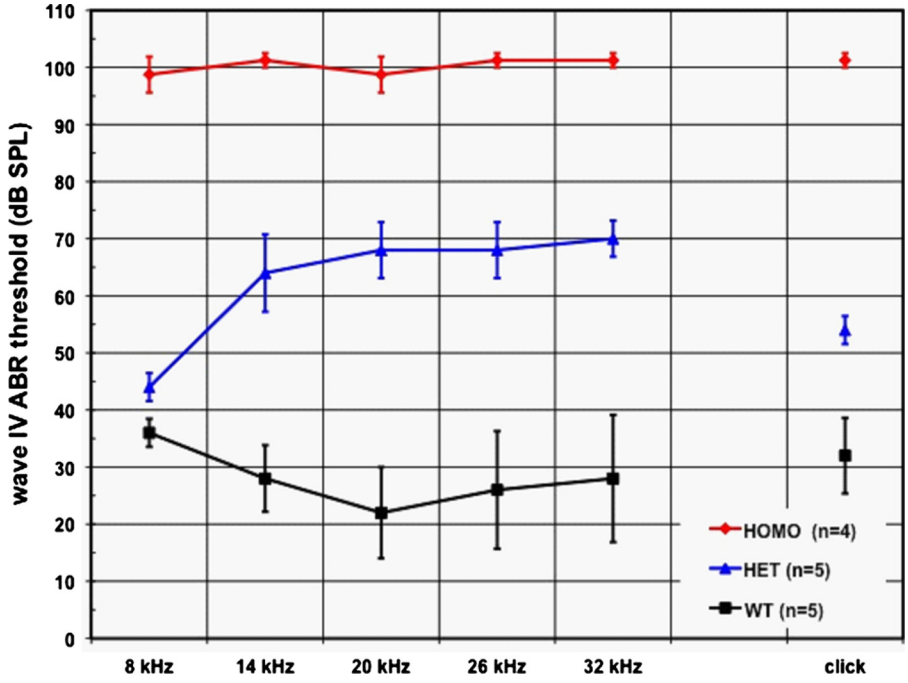

FIGURE 2. **ABR audiograms for click and tone bursts at 8–14-20–26-32 kHz obtained from wild type (*black line*), heterozygous (*blue line*), and homozygous (*red line*) *Tommy* mice aged between P18 and P45.** *Bars* represent S.D. Note that click responses are plotted at an arbitrary point on the frequency axis (the position does not reflect the frequency content of click stimuli).

Affected N4 backcross progeny were intercrossed to investigate potential homozygous phenotypes. Resultant litters produced animals with more severe phenotypes at frequencies consistent with them being *Tmy*/*Tmy* homozygotes (22% displayed an enhanced phenotype, total progeny $n = 65$). Such animals were visibly smaller than their littermates and failed to exhibit any response to click-box analysis from birth, indicating a profound congenital deafness. In addition these animals were severely ataxic, displaying a hesitant wobbly gait with frequent hyperextension of the rear limbs.

Genetic Mapping and Candidate Screening—Using semi-automated fluorescent genome wide linkage analysis, we initially positioned the *Tmy* locus within a ~30-centimorgan region of mouse chromosome 6 flanked by polymorphic microsatellite markers *D6Mit67* and *D6Mit295*. An additional 78 affected heterozygous animals were used to refine the initial region of linkage to a 1.5-centimorgan critical region between markers *D6Mit287* and *D6Mit366*. This 3.1-Mb chromosomal segment is predicted by ENSEMBL to contain 36 known genes including the *Atp2b2* locus. Given the substantial overlap displayed between the phenotypes of *Tmy/Tmy* and *Atp2b2*$^{dfw/dfw}$ animals, the *Atp2b2* locus became the focus of a mutation screen. Direct sequence analysis of the *Atp2b2* locus revealed a single nucleotide change in exon 7 corresponding to a non-conservative G1750A transition in the full-length coding sequence. This mutation was not seen in either BALB/c or C3H/HeN homozygote control DNAs and is predicted to result in a E584K (with numeration referring to PMCA2 *z/b* pump and corresponding to position 629 in the *w/a* variant, which is the variant present in the hair cells, as mentioned in the Introduction).

Hearing Impairment in Tommy Mutant Mice—Hearing in *Tommy* mice was quantified by monitoring ABRs (see "Experimental Procedures"), which are electrical signals evoked from the brainstem after the presentation of sound stimuli (Fig. 1). We measured the IV wave ABR thresholds for click and tone burst (8–14-20–26-32 kHz) stimuli in wild type, heterozygous, and homozygous *Tommy* mutant mice aged between P18 and P45 (Fig. 2). Profound hearing impairment was found in the homozygote from P18. Measurements at younger stages were not performed due to limitations intrinsic in the ABR technique. A significant difference ($p < 0.001$, $n = 5$) between wild type and *Tommy* heterozygote thresholds was observed with clicks as well as tone bursts at frequencies of 14 kHz and above.

PMCA2w/a Expression and Function in Model Cells—We investigated the effect of the replacement of a glutamic acid with a lysine at position 584 in the PMCA2 *z/b* sequence (corresponding to posi-

A

```
                                        E584
                                         ↓
Hs PMCA2            F R M Y S K G A S E I V L K K C C K I L
Rm PMCA4            F R M Y S K G A S E I I L R K C N R I L
Mm PMCA2            F R M Y S K G A S E I V L K K C C K I L
Mm PMCA4            F R M F S K G A S E I M L R R C D R I L
Rn PMCA2            F R M Y S K G A S E I V L K K C C K I L
Pt PMCA1            Y R I F S K G A S E I I L K K C F K I L
Bt PMCA1            Y R I F S K G A S E I I L K K C F K I L
Ss PMCA1            Y R I F S K G A S E I I L K K C F K I L
Oc PMCA1            F R I F S K G A S E I I L K K C F K I L
Rc PMCA1            Y R M F S K G A S E I L L K K C S R I L
Xl PMCA3            F R M Y S K G A S E I I L K K C S R I L
Dr PMCA4            F R M Y S K G A S E I V L R K C S H I L
Pc PMCA3            F R I Y S K G A S E I V L K K C S Q I L
Ce PMCA3            Y R V F S K G A S E I V T K R C K Y F L
Eh PMCA             I R M F T K G A P E M I L E K C Q Y Y M
Dd P-type ATPase    L I I Y V K G A A E I V L N N C T N I V
```

B

```
                                        E584
                                         ↓
Hs PMCA1            F R L F S K G A S E I L L K K C T N I L
Hs PMCA2            F R M Y S K G A S E I V L K K C C K I L
Hs PMCA3            F R I F S K G A S E I I L K K F C K I L
Hs PMCA4            F R M F S K G A S E I M L R R C D R I L
Hs SERCA1           N K M F V K G A P E G V I D R C N Y V R
Hs SERCA2           - K M F V K G A P E S V I E R C S S V R
Hs SERCA3           S K M F V K G A P E S V I E R C S S V R
Hs SPCA1            E I C F M K G A Y E O V I K Y C T T Y N
Hs Na+/K+ ATPase    H V L V M K G A P E R I L D R C S T I L
Hs H+/K+ ATPase     F L M V M K G A P E R I L E K C S T I M
```

FIGURE 3. **Sequence alignment of several PMCA family members showing E584 is highly conserved.** Similarity analysis was performed using the ClustalW program. Human PMCA2 sequence is listed (GenBank™ accession number NP_001674) with other PMCAs sequences from other species (*A*) and with those of other P-type human (*Hs*) ATPases (*B*) GenBank™ accession numbers AY928176 (Rhesus Macaque (*Rm*), PMCA4), AAH75643 (*Mus musculus* (*Mm*), PMCA2), BC109173 (*M. musculus*, PMCA4), NP_036640 (*Rattus norvegicus* (*Rn*), PMCA2), XP_509257 (*Pan troglodytes* (*Pt*), PMCA1), NP_777121 (*Bos taurus* (*Bt*), PMCA1), NP_999517 (*Sus scrofa* (*Ss*), PMCA1), Q00804 (*Oryctolagus cuniculus* (*Oc*), PMCA1), AAK11272 (*Rana catesbeiana* (*Rc*), PMCA1), AAH77905 (*Xenopus laevis* (*Xl*), PMCA3), EU559285 (*Dario rerio* (*Dr*), PMCA4); AAR28532 (*Procambarus clarkia* (*Pc*), PMCA3), AAK68551 (*Caenorhabditis elegans* (*Ce*), PMCA3), XP_653525 (*Entamoeba histolytica* (*Eh*)), EAL62716 (*Dictyostelium discoideum* (*Dd*)), NP_001001323 (PMCA1), NP_068768 (PMCA3), NP_001675 (PMCA4), NP_004311 (SERCA1), NP_733765 (SERCA2), NP_777615 (SERCA3), AAF35375 (SPCA1), NP_000693 (Na^+/K^+ ATPase) and AAH31609 (H^+/K^+ ATPase).

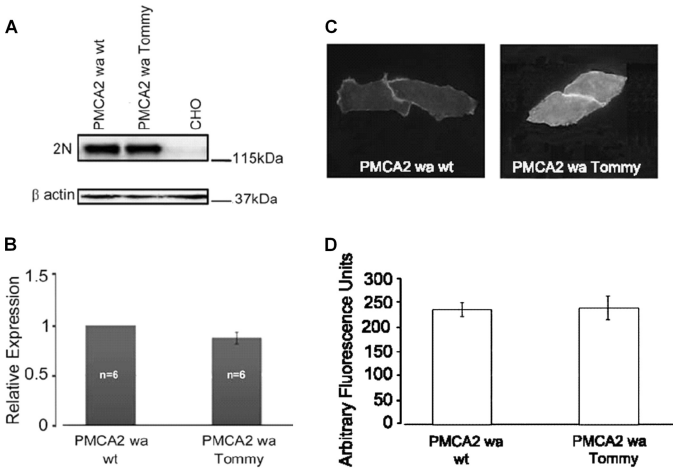

FIGURE 4. **Expression and immunolocalization of recombinant PMCA2*w/a* pumps in CHO cells.** *A*, Western blotting analysis is shown. The band of ~130 kDa corresponds to PMCA2, and the band of ~42 kDa corresponds to β-actin. *B*, densitometric analysis of relative expression of wild type PMCA2*w/a* and PMCA2*w/a* harboring the *Tommy* mutation is shown. The amounts of pump protein were as normalized for β-actin. *C*, immunolocalization of wild type (*left*) and *mutant (right*) PMCA2*w/a* in transiently transfected CHO cells is shown. The interaction with the 2N antibody was probed by the AlexaFluor488-conjugated secondary antibody. *D*, fluorescence levels in the plasma membrane is quantified as described under "Experimental Procedures." *Bars* represent S.D.

tion 629 in the *w/a* variant) using an expression system in model cells. As documented in Fig. 3, the corresponding Glu-584 residue of PMCA2*z/b* is well conserved among the PMCA isoforms in different species (*panel A*) and different Ca^{2+} pumps (*panel B*). The wild type mammalian PMCA2*w/a* protein or the E629K mutant were overexpressed in CHO cells. We verified by Western blotting analysis that transfected cells expressed equal levels of wild type and mutant pumps (Fig. 4, *A* and *B*). We also verified by immunocytochemistry that the overexpressed pumps were correctly delivered to the plasma membrane in equivalent amounts (Fig. 4, *C* and *D*). To monitor Ca^{2+} transients, CHO cells co-transfected with the cDNA encoding the cytosolic Ca^{2+} sensitive photoprotein aequorin (cytAEQ) were stimulated with the purinergic agonist ATP to evoke inositol trisphosphate-mediated cytosolic Ca^{2+} increases. As shown in Fig. 5, *A* and *B*, essentially no differences were detected between the two pump variants in the immediate response to the sudden increase of Ca^{2+} induced by ATP stimulation. Thus, the Ca^{2+} peak was 3.16 ± 0.25 μM ($n = 15$) in cells overexpressing wild type PMCA2 *w/a*, 3.01 ± 0.27 μM ($n = 15$) in those overexpressing the *Tommy* mutation (E629K) and 3.06 ± 0.17 μM ($n = 6$) in control cells (Fig. 5*B*). However, the mutation significantly affected ($p < 0.001$), the declining phase of the Ca^{2+} transient that represented the recovery to basal Ca^{2+} levels (Fig. 5*C*). Namely, the half-time of the declining phase was 61.8 ± 7.85 s ($n = 6$) in control cells, 6.77 ± 0.6 s ($n = 13$) in those overexpressing the wild type pump, and 39.38 ± 6.71s ($n = 14$) in those overexpressing the mutant pump.

PMCA2 Expression and Function in Vestibular Hair Cells of P6-P7 Tommy Mice—The PMCA2 ability to extrude Ca^{2+} was then investigated *in situ* using neonatal (P6-P7) organotypic cultures of utricle sensory epithelium. The choice of utricles was dictated on the one hand by the larger dimension of the sensory hair bundle in vestibular hair cells compared with cochlear hair cells and on the other hand by the greater ease with which the utricular preparation can be fixed to the coverslip to acquire confocal images with the cell main axis resting in the focal plane (Fig. 6, *A–C*). Hair cells in this preparation were stimulated by the rapid photorelease of Ca^{2+} from a cytosolic-caged precursor (*o*-nitrophenyl-EGTA, Fig. 6*D*). The hair cell dissipate this sudden increase of $[Ca^{2+}]_i$ by the action of endogenous buffers, uptake by mitochondria (11), and transport by Ca^{2+}-ATPases (15). The PMCA2*w/a* isoform is present at very high concentration in the hair cell stereocilia (11, 22, 32). To quantify the recovery of $[Ca^{2+}]_i$ after the UV flash, we used the time constant τ of a single-exponential fit (Fig. 6*D*, *red dashed line*) to the $\Delta f/f_0$ trace obtained by spatially averaging the Ca^{2+} transient within the stereocilia compartment. The ability of PMCA2 to extrude Ca^{2+} depends among other things also on the $[Ca^{2+}]_i$ levels; thus, we decided to select only experiments with similar $\Delta f/f_0$ transients (Fig. 6*E*, *left panel*). In wild type mice, the recovery to base line $[Ca^{2+}]_i$ was faster (τ = 2.78 ±

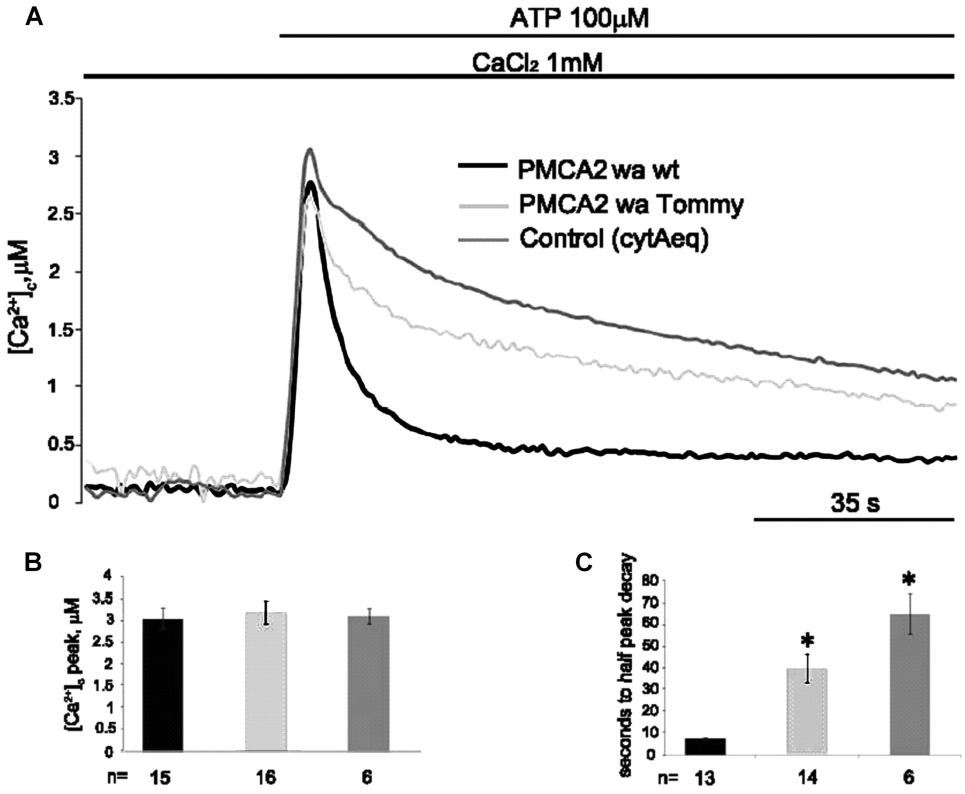

FIGURE 5. **Activity of recombinant PMCA2 pumps in CHO cells.** *A*, cells were transiently either co-transfected with the PMCA2 variants and cytosolic Ca^{2+}-sensitive photoprotein aequorin (*cytAEQ*) or with cytAEQ alone (*Control*). They were then perfused with KRB supplemented with 1 mM $CaCl_2$. 100 μM ATP was used to produce a transient cytosolic Ca^{2+} increase. *B* and *C*, histograms show the means of Ca^{2+} peaks and the half-peak decay times, respectively (*n* indicates the number of experiments considered for the statistical analysis). *, $p < 0.01$ calculated with respect to the wild type pump. *Bars* represent S.D.

0.27 s, $n = 11$ cells from m = 3 mice) than in heterozygous ($\tau = 3.80 \pm 0.80$ s, $n = 11$, m = 3; *, $p = 0.21$, one-way analysis of variance) and, especially, homozygous *Tommy* mice ($\tau = 4.47 \pm 0.87$ s, $n = 18$, m = 4; **, $p = 0.12$, one-way analysis of variance) (Fig. 6*E*, *right panel*).

PMCA2 Expression in Situ and Organ of Corti Degeneration—We performed confocal imaging immunoassays in the neonatal utricle preparation using antibodies selective for the PMCA2 (Fig. 7). P7 utricle cultures from wild type, heterozygous, and homozygous *Tommy* mice presented with selective localization of the PMCA2 in the plasma membrane of the stereocilia with comparable levels of fluorescence. Although not quantitative, these results suggest that the differences in recovery after Ca^{2+} photoliberation highlighted above reflected a dysfunction of the pump more than problems with its expression or targeting.

Immunofluorescence was also used to monitor the progressive degeneration of the organ of Corti, which correlates with the lack of auditory function in the homozygote (Fig. 2). By immunolabeling transversal and orthogonal sections of the cochlea, we observed a progressive base to apex loss of PMCA2 in the hair cells of homozygous *Tommy* mice after P40 (Figs. 8 and 9). At P60, PMCA2 immunofluorescence signal was virtually absent in the basal part of the cochlea, and signs of hair cell degeneration were evident by the lack of several nuclei stained with DAPI.

DISCUSSION

The *Tommy* mouse mutation described here was identified as a new PMCA2 pump mutant with progressive deafness from an ENU mutagenesis screen. It is the 4th PMCA2 point mutation so far found to be linked to hereditary hearing loss in mice. Other deafness-related mutations in the mouse *Atp2b2* gene have been described that led in some cases to the truncation of the molecule and to its eventual disappearance from the stereocilia of hair cells (15, 18, 26). Three of the described mutations were instead point mutations that did not compromise the reading frame of the gene and were, thus, compatible with the expression of the full-length PMCA2*w/a* variant of the pump; they all affected residues that are highly conserved in all PMCA isoforms across species and in other P-type pumps. The original *deaf-waddler* mutation was a Gly-Ser replacement at position 283 in the first cytosolic loop of the pump (17). A second unnamed mutation was a Thr-Lys substitution at position 692 (737 in the *w/a* variant) in the C-terminal half of the large cytosolic loop that connects transmembrane domains 4 and 5 of the molecule (24). In the *Oblivion* mutation a Ser was replaced by a Phe at position 877 (position 922 in the *w/a* variant) in the 6th transmembrane domain of the pump (25).

Recent work has indicated that the amount of Ca^{2+} entering through the MET channels corresponds to only ~0.2% of the total inward current (11). Thus, with K^+ as the monovalent cation driven by the endolymphic potential and with an estimated ~40% MET channels open at rest, the Ca^{2+} fraction of the total MET current *in vivo* should correspond to 3 pA in apical OHCs. The maximum Ca^{2+} load when all MET channels are gated open is estimated to correspond to a current of 7 pA. Both figures are well within the maximal clearing rate estimated for a density of ~6000/μm^2 PMCA2 pumps, which, assuming a conservative turnover rate of 100 ions/s as measured in erythrocytes (33), could safely clear a sustained influx corresponding to a current of 20 pA (11). However, OHCs in the basal (high frequency) region of the cochlea may have to cope with 5-fold larger currents through MET channels (34, 35). Other things being equal, the larger Ca^{2+} load could exceed the extrusion capacity of the PMCA2 in these cells. Therefore, mutations that decrease this capacity might completely disrupt Ca^{2+} homeostasis, with the basal turn of the cells more severely affected than the apex and with OHCs more affected than inner hair cells, as found in both the *Oblivion* and *Tommy* mice. A dimin-

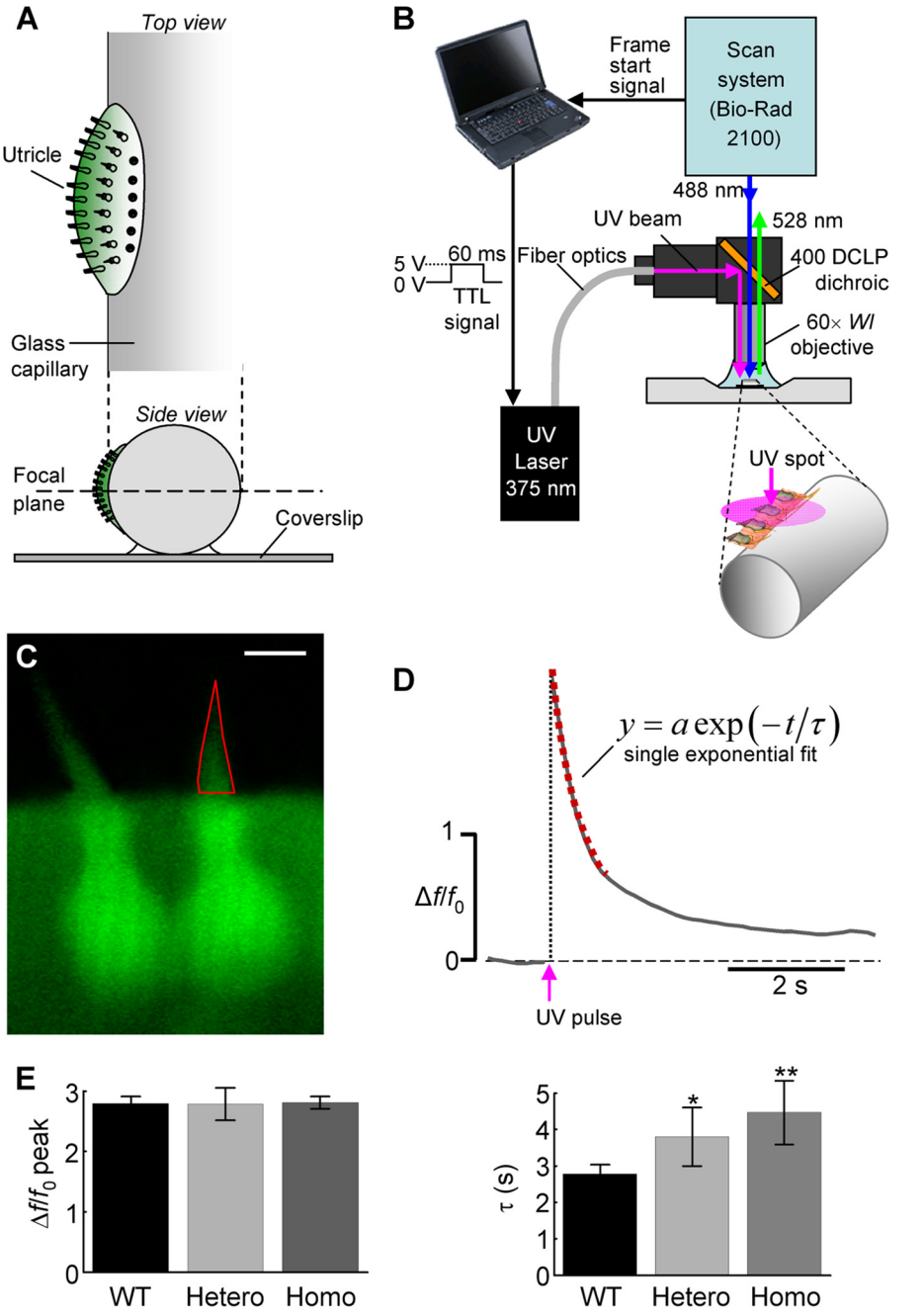

FIGURE 6. **Activity of native PMCA2w/a pumps in vestibular hair cells.** *A*, utricle fixation to the lateral side of a glass capillary permits observation of hair cells along their main axis, thus, to better estimate $[Ca^{2+}]_i$ changes both in the hair cell stereocilia and body compartments. *B*, UV laser light (375 nm), controlled by a transistor-transistor logic signal generated by a computer connected to the Bio-Rad 2100 scanning system, was delivered for 60 ms to elicit a homogeneous $[Ca^{2+}]_i$ increase in an area covering a few hair cells. *TTL*, transistor-transistor logic; *WI*, water immersion. *C*, Fluo-4 absolute fluorescence *f*, peaked at 515 nm, is shown *green color-coded* (*scale bar*, 5 μm). The averaged *f* in the stereociliary compartment (bounded by the *red line*) was used to compute the $[Ca^{2+}]_i$ change parameter $\Delta f/f_0$. *D*, a representative $\Delta f/f_0$ stereociliary time course (UV flash delivered at time indicated by the *violet arrow*) is shown for a wild type *Tommy* mouse. The decay time constant τ of the single-exponential curve (*red dashed line*) fitting the $\Delta f/f_0$ trace after the UV flash was used to quantify Ca^{2+} clearance rate from the stereocilia. *E*, the experiments were selected to have similar $\Delta f/f_0$ transients (*left panel*). In wild type (*WT*) mice, the recovery to base-line Ca^{2+} was faster (*right panel*, $\tau = 2.78 \pm 0.27$ s, means ± S.E., $n = 11$ from 3 mice) than in the heterozygous ($\tau = 3.80 \pm 0.80$ s, $n = 11$ from 3 mice; *, $p = 0.21$ in the analysis of variance test) and in the homozygous *Tommy* mice ($\tau = 4.47 \pm 0.87$ s, $n = 18$ from 4 mice; **, $p = 0.12$ in the analysis of variance test).

ished Ca^{2+} removal from the cells is also expected to affect the MET currents. Indeed, the pharmacological blockade of the PMCA2 pump shifted the current-displacement (*I-X*) curve in the positive direction and reduced its slope considerably (11). Similar effects have been reported by mutation or knock out of the PMCA2 isoform of the plasma membrane Ca^{2+} pump (23).

The only cochlear PMCA2 exposed to endolymph is that of the stereocilia (36, 37). Thus, if less Ca^{2+} is exported from the stereocilia, as occurs in the PMCA2 mutants discussed here, its concentration in the endolymph is expected to fall (37). This may provide a clue as to why in some cases mutations in the gene of the PMCA2 pump potentiated the deafness phenotype induced by co-existing mutations of cadherin-23 (USH1D), a single pass membrane Ca^{2+}-binding protein that is abundantly expressed in the stereocilia. Cadherin-23 has a prolonged extracellular portion exposed to the endolymph that contains 27 cadherin (Ca^{2+} binding) domains (38). Its homodimers interact in *trans* with homodimers of protocadherin-15 (USH1F), another cadherin that has 15 external cadherin domains (39). Both cadherins are defective in Usher syndrome type I (sensorineural deafness and blindness due to retinitis pigmentosa). The two cadherins interact together and form transient lateral links interconnecting the stereocilia and anchor to the stereocilia actin filaments (40), which provide the initial cohesion of the developing hair bundle. After completion of hair bundle morphogenesis, cadherin-23 and protocadherin-15 form the upper and lower parts of the tip link, respectively, *i.e.* the molecular machinery of the MET complex is anchored to the cytoplasmic region of protocadherin-15 (39, 41).

Recent work (38) has solved the three-dimensional structure of the first two repeats of cadherin-23, which show typical cadherin folds with an elongated N terminus, which contributes to forming the N-terminal Ca^{2+} binding site. The interaction of Ca^{2+} with binding sites in cadherin-23 is critical to the function of the tip links. A reduced concentration of endolymphic Ca^{2+} has been

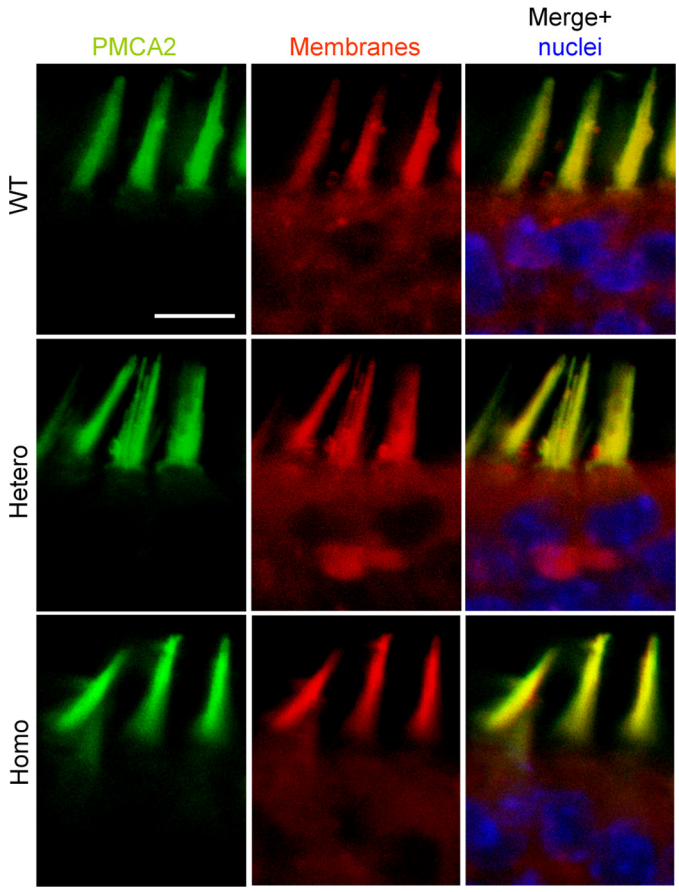

FIGURE 7. **PMCA2 immunolabeling in neonatal utricle.** Confocal imaging immunoassays of PMCA2 (stained by Alexa 488 conjugated, *green*) in P7 utricle cultures from wild type, heterozygous, and homozygous *Tommy* mice (for details see "Experimental Procedures"). Membranes (*red*) are stained by FM4-64FX, whereas nuclei (*blue*) are stained by DAPI. *Scale bar*, 10 μm.

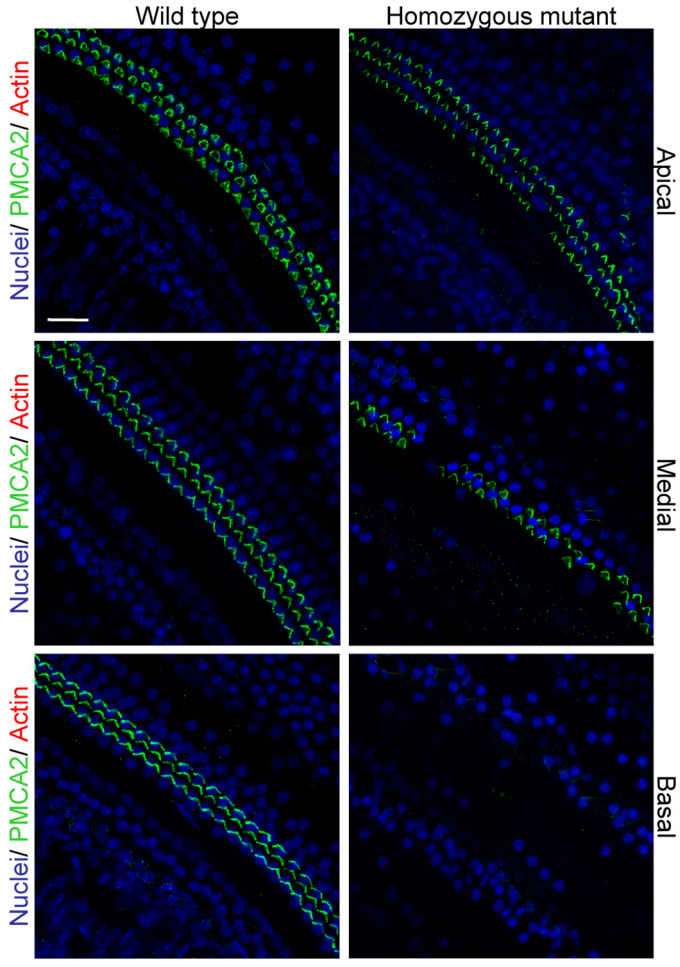

FIGURE 8. **PMCA2 immunolabeling in P60 cochlea whole mounts.** Horizontal sections (orthogonal to the modiolus) of cochlea whole mounts from P60 wild type (*left column*) and homozygous (*right column*) *Tommy* mice are shown. Images from apical, medial, and basal regions are obtained by maximal back-projection of 20 confocal optical sections from a 2-μm step z-stack of wild type and homozygous *Tommy* mice. PMCA2 expression was probed by a PMCA2 selective antibody (Alexa 488 conjugated, *green*), and nuclei were stained with DAPI (*blue*). *Scale bar*, 15 μm.

found to affect the degree of their stiffness, which is required for the opening of the MET channels, even possibly leading in extreme cases to their disappearance (42). The Ca^{2+} affinity of the cadherin-23 fragment, estimated from models with three or four Ca^{2+} binding sites, corresponded to K_D values increasing from 1.9 to 71.4 μM, *i.e.* in the range of the Ca^{2+} concentration in the endolymph. Molecular dynamics simulations suggested the repeats to be stiff; removal of Ca^{2+}, which is known to abolish the MET currents (42, 43), reduced the rigidity, which was also decreased by reducing the affinity of the binding sites for Ca^{2+}. This occurred in the deafness-inducing cadherin-23 mutant D101G, which was modeled using three Ca^{2+} binding sites, and in which the K_D values for Ca^{2+} increased from 3.9 μM to more than 100 μM. The degree of rigidity and the unfolding strength of cadherin-23 were, thus, critically sensitive to the concentration of Ca^{2+} in the environment, *i.e.* in the endolymph, whose value in the bulk is poised at ~20 μM by the Ca^{2+} export function of the PMCA2 pump (higher values, up to about 50 μM, might, however, be present in the immediate proximity of the MET channels) (44).

The cooperation of the cadherin-23 and the PMCA 2 pump is evidently critical in the molecular events that ultimately permit the neural encoding of the acoustic signal. It is, thus, easy to appreciate the importance of their mutations in the generation of the hearing loss phenotype; indeed, a G753A polymorphism of cadherin-23 was detected in the original *deafwaddler* mice (45). Furthermore, in one human family a homozygous mutation in cadherin-23 (F1888S) caused the hearing loss in five siblings, whereas a co-existent heterozygous PMCA2 pump mutation (V586M in the *z/b* nomenclature) was associated with increased loss in the three most severely affected siblings (27). In another human family in which both parents had normal hearing, a Thr → Ser substitution at position 1999 was detected in the cadherin-23 of the father but not in that of the mother, who presented instead with the G293S mutation of the PMCA2 pump. It is noteworthy that the G293S mutation of PMCA2 involved the same couple of residues of the original *deafwaddler* mutation and occurred 10 residues downstream of the mouse residue. One son, affected by severe bilateral hearing impairment without vestibular involvement, inherited both mutations, whereas a brother with normal hearing was negative for the G293S mutation like the father (23). The link between cadherin-23 and the PMCA2 pump, therefore, is important. However, it is not obligatory, as shown by the results of the

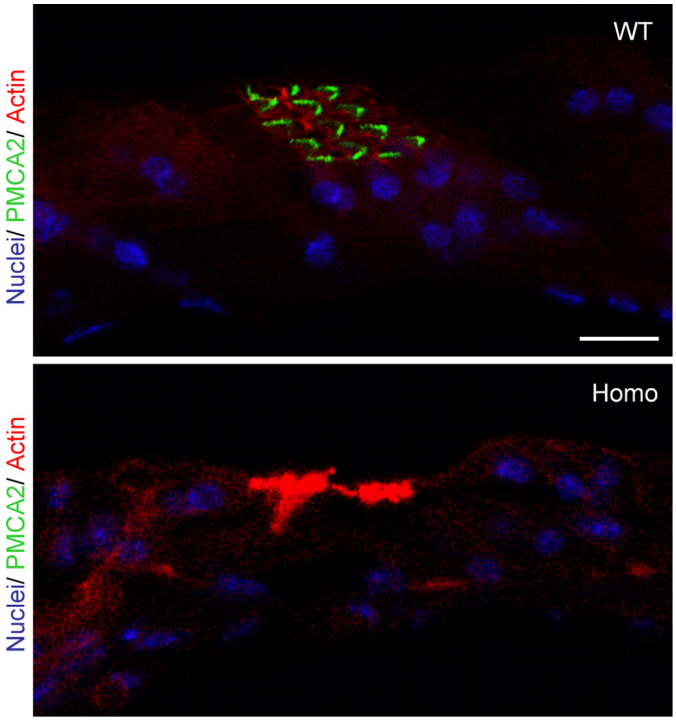

FIGURE 9. **PMCA2 immunolabeling in basal cochlear transversal sections (parallel to the modiolus) of P60 Tommy mice.** Images were obtained by maximal back-projection of 2–6 confocal optical sections from a 1-μm step z-stack of wild type (*top panel*) and homozygous (*bottom panel*) *Tommy* mice. Actin filaments were stained with phalloidin (Texas Red-conjugated, *red*) and nuclei with DAPI (*blue*). *Scale bar*, 15 μm.

Tommy mutant described here and those on the *Oblivion* mutant (25). Evidently, the biochemical defect of the homeostasis of Ca^{2+} in the stereocilia of OHCs has different degrees of severity. Homozygous cadherin-23 mutations that impair the ability of the protein to bind Ca^{2+}, as detected in one of the human families described (27), may be sufficient to disrupt the opening properties of the MET channels, generating the hearing loss phenotype, which is then only exacerbated by the concomitant PMCA2 pump mutation. On the other hand, homozygous PMCA2 pump mutations, as was the case for the *Oblivion* mutant and is the case for the *Tommy* mutant, may *per se* be sufficient to decrease the Ca^{2+} concentration in the endolymph to a degree that would affect the function of the otherwise normal cadherin-23 in the tip links and to generate the hearing loss phenotype without the contribution of cadherin-23 mutations.

The *Tommy* mutation (E584K in the *z/b* nomenclature) affects a highly conserved residue located in the second intracellular loop of the pump only two residues upstream the site of the conservative mutation reported in Ficarella *et al.* (23). Based on the nearly identical position in the sequence (both residues are located in the domain that binds ATP), it could have been expected that the mutations would have the same effect on the hearing phenotype. However, the character of the replacement in the *Tommy* mutation (E/K) is much more dramatic than the human V586M conservative substitution. In principle, thus, it could be expected that the defect of the pump in the *Tommy* mutant would be more severe. The effect of the human V586M mutation on the PMCA2 pump has only been defined as a decrease of the pumping activity, although molecular modeling of the V586M replacement on a SERCA pump template had suggested structural disturbances of the ATP binding site by the presence of the sterically larger methionine side chain. It would, thus, be useful to analyze the V586M in the same molecular detail as the *Tommy* mutant.

The results presented here showing a reduced Ca^{2+}-pumping ability of the *Tommy* mutant PMCA2 and the discussion of the PMCA2 and cadherin-23 mutants underline the importance of the concerted functioning of the two molecules for the neural encoding of acoustic stimuli. They show that the special properties of the variant of the PMCA2 pump of the stereocilia are a critical factor; the ability of the pump to export Ca^{2+} at a constant level essentially irrespective of the presence of activators, *e.g.* calmodulin, which is present in the stereocilia (46) at a concentration of ~70 μM (47), ensures that the endolymph will be continuously replenished with Ca^{2+} to compensate for the (minor) amount that enters into the stereocilia. This in turn ensures the correct functioning of the tip-links-MET channel machinery. The discussion has concentrated on the interplay between the PMCA2 pump and cadherin-23: possibly, however, PMCA2 pump defects could have much wider importance; *i.e.* they could act as modifiers of other hearing loss phenotypes, genetic and/or environmental, characterized by pathological processes affecting hair cells (27).

REFERENCES

1. Gillespie, P. G., and Müller, U. (2009) *Cell* **139,** 33–44
2. Dallos, P., Wu, X., Cheatham, M. A., Gao, J., Zheng, J., Anderson, C. T., Jia, S., Wang, X., Cheng, W. H., Sengupta, S., He, D. Z., and Zuo, J. (2008) *Neuron* **58,** 333–339
3. Ashmore, J. (2008) *Physiol. Rev.* **88,** 173–210
4. Mammano, F., and Ashmore, J. F. (1993) *Nature* **365,** 838–841
5. Nobili, R., and Mammano, F. (1996) *J. Acoust. Soc. Am.* **99,** 2244–2255
6. Fuchs, P. A. (2005) *J. Physiol.* **566,** 7–12
7. Pickles, J. O., Comis, S. D., and Osborne, M. P. (1984) *Hear. Res.* **15,** 103–112
8. Beurg, M., Fettiplace, R., Nam, J. H., and Ricci, A. J. (2009) *Nat. Neurosci.* **12,** 553–558
9. Denk, W., Holt, J. R., Shepherd, G. M., and Corey, D. P. (1995) *Neuron* **15,** 1311–1321
10. Ricci, A. J., and Fettiplace, R. (1998) *J. Physiol.* **506,** 159–173
11. Beurg, M., Nam, J. H., Chen, Q., and Fettiplace, R. (2010) *J. Neurophysiol.* **104,** 18–34
12. Bosher, S. K., and Warren, R. L. (1978) *Nature* **273,** 377–378
13. Hackney, C. M., Mahendrasingam, S., Penn, A., and Fettiplace, R. (2005) *J. Neurosci.* **25,** 7867–7875
14. Crouch, J. J., and Schulte, B. A. (1995) *Hear. Res.* **92,** 112–119
15. Kozel, P. J., Friedman, R. A., Erway, L. C., Yamoah, E. N., Liu, L. H., Riddle, T., Duffy, J. J., Doetschman, T., Miller, M. L., Cardell, E. L., and Shull, G. E. (1998) *J. Biol. Chem.* **273,** 18693–18696
16. Noben-Trauth, K., Zheng, Q. Y., Johnson, K. R., and Nishina, P. M. (1997) *Genomics* **44,** 266–272
17. Street, V. A., McKee-Johnson, J. W., Fonseca, R. C., Tempel, B. L., and Noben-Trauth, K. (1998) *Nat. Genet.* **19,** 390–394
18. Takahashi, K., and Kitamura, K. (1999) *Biochem. Biophys. Res. Commun.* **261,** 773–778
19. Brini, M., Coletto, L., Pierobon, N., Kraev, N., Guerini, D., and Carafoli, E. (2003) *J. Biol. Chem.* **278,** 24500–24508
20. Hilfiker, H., Guerini, D., and Carafoli, E. (1994) *J. Biol. Chem.* **269,** 26178–26183
21. Hill, J. K., Williams, D. E., LeMasurier, M., Dumont, R. A., Strehler, E. E., and Gillespie, P. G. (2006) *J. Neurosci.* **26,** 6172–6180

22. Grati, M., Aggarwal, N., Strehler, E. E., and Wenthold, R. J. (2006) *J. Cell Sci.* **119,** 2995–3007
23. Ficarella, R., Di Leva, F., Bortolozzi, M., Ortolano, S., Donaudy, F., Petrillo, M., Melchionda, S., Lelli, A., Domi, T., Fedrizzi, L., Lim, D., Shull, G. E., Gasparini, P., Brini, M., Mammano, F., and Carafoli, E. (2007) *Proc. Natl. Acad. Sci. U.S.A.* **104,** 1516–1521
24. Tsai, Y. S., Pendse, A., Moy, S. S., Mohri, I., Perez, A., Crawley, J. N., Suzuki, K., and Maeda, N. (2006) *Mamm. Genome* **17,** 716–722
25. Spiden, S. L., Bortolozzi, M., Di Leva, F., de Angelis, M. H., Fuchs, H., Lim, D., Ortolano, S., Ingham, N. J., Brini, M., Carafoli, E., Mammano, F., and Steel, K. P. (2008) *PLoS Genet* **4,** e1000238
26. McCullough, B. J., and Tempel, B. L. (2004) *Hear. Res.* **195,** 90–102
27. Schultz, J. M., Yang, Y., Caride, A. J., Filoteo, A. G., Penheiter, A. R., Lagziel, A., Morell, R. J., Mohiddin, S. A., Fananapazir, L., Madeo, A. C., Penniston, J. T., and Griffith, A. J. (2005) *N. Engl. J. Med.* **352,** 1557–1564
28. Isaacs, A. M., Davies, K. E., Hunter, A. J., Nolan, P. M., Vizor, L., Peters, J., Gale, D. G., Kelsell, D. P., Latham, I. D., Chase, J. M., Fisher, E. M., Bouzyk, M. M., Potter, A., Masih, M., Walsh, F. S., Sims, M. A., Doncaster, K. E., Parsons, C. A., Martin, J., Brown, S. D., Rastan, S., Spurr, N. K., and Gray, I. C. (2000) *Hum. Mol. Genet* **9,** 1865–1871
29. Hardisty-Hughes, R. E., Parker, A., and Brown, S. D. (2010) *Nat. Protoc.* **5,** 177–190
30. Brini, M., Marsault, R., Bastianutto, C., Alvarez, J., Pozzan, T., and Rizzuto, R. (1995) *J. Biol. Chem.* **270,** 9896–9903
31. Mammano, F., and Bortolozzi, M. (2010) in *Calcium Measurement Methods* (Verkhratsky, A., and Petersen, O., eds) Vol. 43, pp. 57–80, Humana Press, New York
32. Lumpkin, E. A., and Hudspeth, A. J. (1998) *J. Neurosci.* **18,** 6300–6318
33. Kubitscheck, U., Pratsch, L., Passow, H., and Peters, R. (1995) *Biophys. J.* **69,** 30–41
34. Ricci, A. J., Crawford, A. C., and Fettiplace, R. (2003) *Neuron* **40,** 983–990
35. Beurg, M., Evans, M. G., Hackney, C. M., and Fettiplace, R. (2006) *J. Neurosci.* **26,** 10992–11000
36. Dumont, R. A., Lins, U., Filoteo, A. G., Penniston, J. T., Kachar, B., and Gillespie, P. G. (2001) *J. Neurosci.* **21,** 5066–5078
37. Wood, J. D., Muchinsky, S. J., Filoteo, A. G., Penniston, J. T., and Tempel, B. L. (2004) *J. Assoc. Res. Otolaryngol.* **5,** 99–110
38. Sotomayor, M., Weihofen, W. A., Gaudet, R., and Corey, D. P. (2010) *Neuron* **66,** 85–100
39. Kazmierczak, P., Sakaguchi, H., Tokita, J., Wilson-Kubalek, E. M., Milligan, R. A., Müller, U., and Kachar, B. (2007) *Nature* **449,** 87–91
40. Petit, C., and Richardson, G. P. (2009) *Nat. Neurosci.* **12,** 703–710
41. Lefèvre, G., Michel, V., Weil, D., Lepelletier, L., Bizard, E., Wolfrum, U., Hardelin, J. P., and Petit, C. (2008) *Development* **135,** 1427–1437
42. Assad, J. A., Shepherd, G. M., and Corey, D. P. (1991) *Neuron* **7,** 985–994
43. Vollrath, M. A., Kwan, K. Y., and Corey, D. P. (2007) *Annu. Rev. Neurosci.* **30,** 339–365
44. Farris, H. E., Wells, G. B., and Ricci, A. J. (2006) *J. Neurosci.* **26,** 12526–12536
45. Noben-Trauth, K., Zheng, Q. Y., and Johnson, K. R. (2003) *Nat. Genet.* **35,** 21–23
46. Furness, D. N., Karkanevatos, A., West, B., and Hackney, C. M. (2002) *Hear. Res.* **173,** 10–20
47. Walker, R. G., Hudspeth, A. J., and Gillespie, P. G. (1993) *Proc. Natl. Acad. Sci. U.S.A.* **90,** 2807–2811
48. Parkinson, N. J., Mackenzie, F., Brooker, D., Fray, M., Glenister, P., and Brown, S. D. M (2003) *The Tommy Mouse Mutant Is a New Allele of dfw That Displays Semi-dominant Age-related Hearing loss*, Association for Research in Otolaryngology, Mt. Royal, NJ, Abstract 9065